

# Portable and Versatile Catheter Robot for Image-Guided Cardiovascular Interventions

Nikhil Tej Kantu , *Student Member, IEEE*, Weibo Gao , *Graduate Student Member, IEEE*, Nitin Srinivasan, Gregory D. Buckner , *Member, IEEE*, and Hao Su , *Senior Member, IEEE*

**Abstract**—Cardiovascular disease remains the primary cause of death worldwide, necessitating the development of advanced endovascular instruments and procedures. These interventional procedures typically involve the use of guide catheters and guidewires, which are navigated through the vasculature under X-ray guidance. However, these procedures expose clinicians to prolonged radiation, posing potential health risks. Recent advances in endovascular catheter robots can mitigate the aforementioned risks by allowing teleoperation, but procedural efficacy has been hindered by their bulky designs that require designated facilities. In addition, these robots have limited compatibility with a wide range of instrument types and diameters, restricting their applicability to specific clinical interventions. To address these unmet needs, we have designed, fabricated, and experimentally validated a portable and versatile 4 degree-of-freedom catheter robot that can manipulate commercially available cardiovascular instruments with diameters ranging from 1 to 9 F. Furthermore, we analytically modeled the drive mechanism of the catheter robot and evaluated its tracking and insertion force and torque performance through experiments. Our portable robot (250 mm × 350 mm × 250 mm) is approximately 90% smaller than most state-of-the-art systems, e.g., Siemens Corindus system (1780 mm × 690 mm × 1170 mm), thanks to our highly integrated direct drive motors, mechatronics design, and modular instrument routing. Experimental evaluations

confirm that the robot can actuate guidewires and guide catheters at clinically relevant force and torque amplitudes, speeds, and bandwidths without risking damage to delicate vascular tissues. The clinical potential of our catheter robot is demonstrated by performing a simulated percutaneous coronary intervention using a 3-D-printed model of the human heart. The portability and versatility of this catheter robot make it applicable to a wide range of cardiovascular procedures to potentially facilitate effective treatments.

**Index Terms**—Cardiovascular intervention, catheter, endovascular disease, friction wheel drive, portable, robotics, versatile.

## I. INTRODUCTION

CARDIOVASCULAR disease poses a significant global health challenge, ranking as the leading cause of mortality worldwide, with an estimated 19 million deaths annually [1]. Endovascular procedures, e.g., transcatheter aortic valve replacement (TAVR), percutaneous coronary intervention (PCI), atrial fibrillation ablation, and endovascular aneurysm repair (see Fig. 1) require deployment and precise positioning of catheters and guidewires. PCI treats diseased coronary arteries using a balloon/stent catheter to expand narrowed arteries [2]. TAVR involves utilizing a microcatheter to replace a damaged valve with a prosthetic valve [3]. Atrial fibrillation ablation involves heat (radiofrequency ablation) or cold (cryoablation) energy to create scars on the heart chambers via ablation catheters, blocking abnormal electrical signals (arrhythmias) [4]. Endovascular repair of aortic aneurysms involves inserting a stent graft through a microcatheter to mitigate aneurysm rupture [5].

These minimally invasive procedures are associated with shorter recovery times, reduced risks of complications, and improved patient outcomes as compared to conventional open surgeries [6]. Despite these benefits, these procedures also present notable challenges, including long procedure times, increased radiation exposure for clinicians, and increased clinical workloads and demands for healthcare facilities. The aforementioned challenges can lead to long-term health issues such as cancer and ergonomic injuries [7], [8], [9].

To address the clinical challenges, researchers have made significant advancements in minimally invasive robotics to enable prostate percutaneous therapy and stereotactic neurosurgery [16], [17], [18], [19], [20]. The potential to improve patient outcomes via robotics paved a path for future magnetic resonance imaging (MRI)-guided robot-assisted surgeries [21],

Received 1 July 2024; revised 12 December 2024; accepted 18 March 2025. Recommended by Technical Editor M. Rakotondrabe and Senior Editor C. Clévy. This work was supported in part by the National Institutes of Health under Grant R01NS141171; in part by the National Science Foundation Future of Work under Grant 2222716; in part by NIH (R18 HS029124); and in part by NCSU Research and Innovation Seed Funding. (Nikhil Tej Kantu and Weibo Gao contributed equally to this work.) (Corresponding author: Hao Su.)

Nikhil Tej Kantu, Weibo Gao, and Nitin Srinivasan are with the Department of Mechanical and Aerospace Engineering, North Carolina State University, Raleigh, NC 27695 USA.

Gregory D. Buckner is with the Department of Mechanical and Aerospace Engineering, Joint NCSU/UNC Department of Biomedical Engineering, North Carolina State University, Raleigh, NC 27695 USA, and also with the University of North Carolina at Chapel Hill, Chapel Hill, NC 27599 USA.

Hao Su is with the Department of Mechanical and Aerospace Engineering, Joint NCSU/UNC Department of Biomedical Engineering, North Carolina State University, Raleigh, NC 27695 USA, and with the University of North Carolina at Chapel Hill, Chapel Hill, NC 27599 USA, and also with the Biomechatronics and Intelligent Robotics Lab, Tandon School of Engineering, New York University, Brooklyn, NY 11201 USA (e-mail: hao.su@nyu.edu).

This article has supplementary material provided by the authors and color versions of one or more figures available at <https://doi.org/10.1109/TMECH.2025.3559911>.

Digital Object Identifier 10.1109/TMECH.2025.3559911

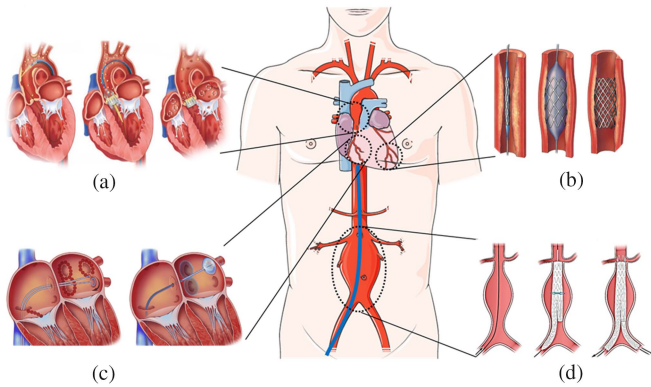


**Fig. 1.** Endovascular interventions for various cardiovascular diseases. (a) Transcatheter aortic valve replacement (TAVR). (b) Percutaneous coronary intervention (PCI). (c) Atrial fibrillation ablation. (d) Endovascular aneurysm repair. These procedures require 2-DoF manipulation of instruments (i.e., rotation and translation) and are typically performed via femoral access and guided by X-ray imaging. Ensuring safe and effective treatment requires employing instruments of varying diameters (0.33–1.00 mm) and working length (100–1200 mm).

[22], [23], [24], [25]. Similarly, for catheter-based endocardial interventions, investigators explored the design optimization of shape memory alloy actuated robotic radiofrequency ablation catheters to augment their performance to address convoluted interventional tasks [26]. Subsequent research focused on path-optimized and closed-loop control of the robotic catheter tip during endocardial ablation [27].

Endovascular catheter robots have been developed and introduced to safeguard clinicians from radiation exposure and musculoskeletal injuries by enabling teleoperated interventions [28], [29], [30], [31], where clinicians use a remote console with improved ergonomic postures. However, the intricate complexities of endovascular interventions pose challenges to the design of catheter robots, which requires enabling a specific range of motion (RoM) for a variety of intervention instruments while maintaining a compact form for minimizing surgical interference. The commercial Amigo Remote Catheter System, for example, uses a 2-degrees-of-freedom (DoF) actuation module to control steerable catheters [10], but its docking-enabled linear stage and constrained RoM limits its clinical adaptability to only a few procedures.

Most prior art catheter robots utilize two types of gross motion to drive instruments: clamping-based axial motion (constrained RoM) and friction wheel drive-based axial motion (unlimited RoM) [31], [32]. These are further divided into the following four actuation combinations [33], [34] that allow for instrument insertion and rotation:

- 1) mechanisms that utilize linear stages for insertion and clamp mechanisms;
- 2) inchworm-based linear actuators for instrument insertion (intermittent feeder) and gear/belt mechanisms for rotation;
- 3) friction-based instrument translation (continuous feeder) and rotary motion via shear friction;
- 4) friction wheel driver (continuous feeder) for instrument insertion with gear/belt trains for instrument rotation.

Clamping-based linear drive mechanisms were developed to mimic the clinician's delivery process and ensure an adequate grip on the instruments. A 4-DoF, MRI-compatible robot that pneumatically translates instruments via inchworm mechanisms and rotates them via spur gear trains is presented in [11]. However, this inchworm mechanism restricts the device's working length and is subject to task-space backlash, posing challenges for continuous actuation. Friction-drive linear actuation may achieve unconstrained working length within a smaller footprint. The Dual-finger Robotic Hand [13] enables the translation of guidewires and balloon/stent catheters via friction rollers and rotation through a shear friction mechanism, mimicking the clinician's thumb and forefinger movements. The Magellan robotic system [12] utilizes a friction-belt drive mechanism to translate and rotate a guidewire, which enables guide catheter steering and translation through a linear stage. Nevertheless, these robots may experience radial slip during instrument rotation, resulting in inaccurate positioning [12], [13]. Siemens Corindus Robotic System [15], [35] enables 3-DoF instrument translation and rotation through motorized roller pairs and a spur gear train. However, this robot is constrained in its instrument working length and can only actuate a limited range of instruments, restricting its adaptation to specific cardiovascular procedures. Furthermore, the Siemens system suffers from a complex intervention workflow that restricts its ability to treat multiple diseased vessels in a single insertion and requires a significant amount of preprocedural planning due to its closed architecture [8], [9], [36].

As shown in Table I, state-of-the-art robot systems tend to be bulky (typically larger than 500 mm), which may cause physical interference with physicians in robot-assisted interventions. The Corindus Robotic System, for example, suffers from limited adoption due to its large footprint (1780 mm × 690 mm × 1170 mm) [15]. Existing robotic systems may also exhibit limitations in the instrument RoM and compatibility with a range of catheters and guidewires [15], hindering their clinical applicability and widespread adoption; these systems are used in only 1% of endovascular interventions due to their adaptation barriers [37]. Attaining high compatibility and versatility with off-the-shelf interventional instruments while maintaining a compact structure requires an innovative mechatronics design strategy.

In this study, we present a novel, actively adjustable clamping mechanism capable of precisely manipulating *off-the-shelf instruments* across broad diameter ranges. Our friction roller-drive module enables unlimited guidewire insertion/retraction RoM, and this module provides enhanced insertion force via a direct drive motor and a linear actuator to minimize slippage. In addition, our friction roller-drive model considers both roller-instrument interactions and boundary conditions of the actuation module to mitigate instrument slippage. This portable catheter robot is based on a novel actuation mechanism, customized *compact motors* and *electronics* (see Fig. 2).

The contributions of this study are as follows. First, we created a novel 4-DoF portable and versatile catheter robot that enables precise translation and rotation of off-the-shelf guide catheters

TABLE I  
COMPARATIVE OVERVIEW OF STATE-OF-THE-ART ENDOVASCULAR ROBOTIC SYSTEMS AND OUR PROPOSED ROBOT

Robot characteristics	Amigo [10]	Imperial [11]	Magellan [12]	DRH [13]	MIT [14]	Siemens [15]	This Work
Portable design	No	Yes	No	Yes	No	No	Yes
Compromised instrument diameters	Yes	No	Yes	Yes	Yes	Yes	No
Actuation	Electric	Pneumatic	Electric	Electric	Magnetic	Electric	Electric
Guide Catheter rotation—DoF #1	$\pm 180^\circ$	$\pm 180^\circ$	$\pm 180^\circ$	N/A	N/A	$\pm 180^\circ$	$\pm 180^\circ$
Guide Catheter translation—DoF #2	$\sim 100$ mm	$\pm 20$ mm (SSL)	$\sim 88$ mm	N/A	N/A	$\sim 100$ mm	300 mm
Guidewire rotation—DoF #3	N/A	$\pm 180^\circ$	$\pm 180^\circ$	$\pm 180^\circ$	$\pm 180^\circ$	$\pm 180^\circ$	$\pm 180^\circ$
Guidewire translation—DoF #4	N/A	$\pm 20$ mm (SSL)	Unlimited	Unlimited	Unlimited	Unlimited	Unlimited
Facilitate microcatheter translation	No	No	No	No	Yes	Yes	Yes
Key limitation	LF, LD	LD, limited SSL	LF	LD	LF	LF	N/A

SSL: Single stroke length (limited range-of-motion), LF: Large footprint, LD: and Limited degrees-of-freedom.

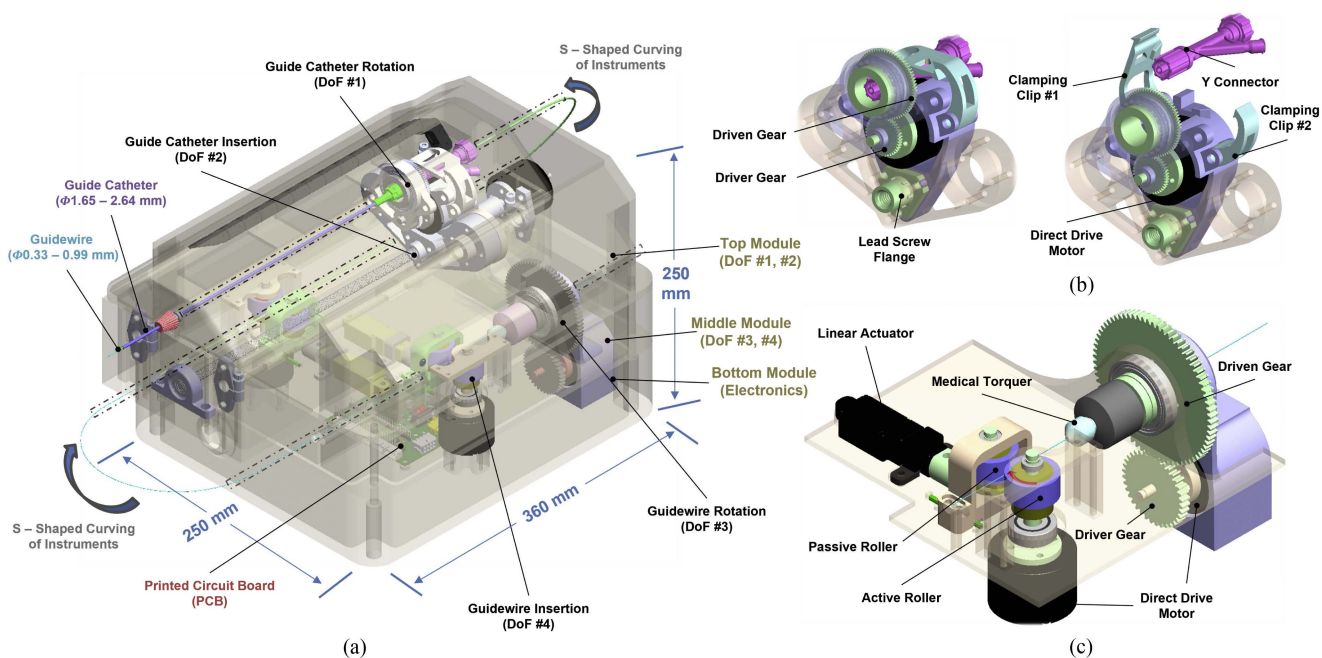
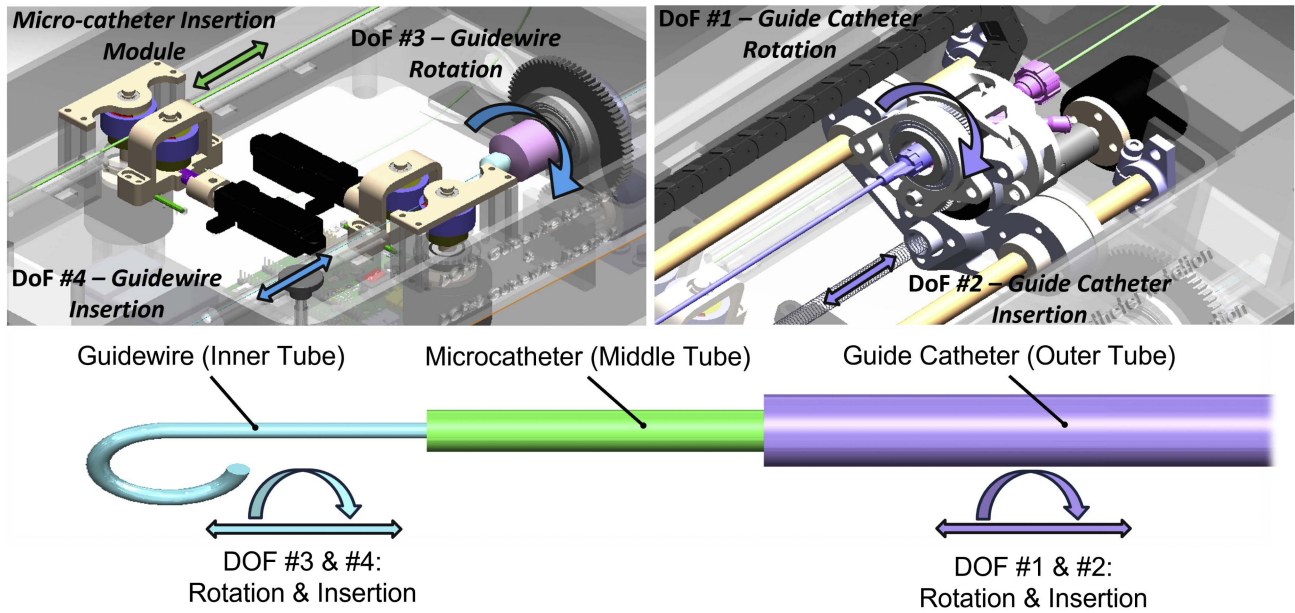


Fig. 2. Mechanics design of our portable and versatile catheter robot. (a) Overview of the 4-DoF robotic system CAD the enclosing top, middle, and bottom modules designed for the actuation of all instruments. (b) 2-DoF guide catheter module: features a lead screw for catheter axial translation and a versatile rotation mechanism, including an adjustable clipping-enabled clamping mechanism to incorporate off-the-shelf Y-connectors to adapt to versatile guide catheters. (c) 2-DoF guidewire module: utilizes a friction roller drive for unconstrained guidewire advancement/retraction range and a medical torquer incorporated into spur gear train for guidewire rotation.

and guidewires within a compact size (250 mm × 350 mm × 250 mm) that is approximately one-tenth the size of the state-of-the-art catheter robots. Second, our actively adjustable clamping mechanism enables the robot to actuate off-the-shelf instruments with diameters ranging from  $\varnothing 0.33$  to  $\varnothing 3$  mm with precise instrument advancement/retraction,  $\pm 0.05$  mm with an unlimited RoM and rotation ( $\pm 0.3^\circ$ ). The portable and versatile capabilities of the robot enhance its practicality in clinical interventions. Benchtop testing results show that our design is a compact robot capable of actuating intervention instruments with the required ranges of motion (linear:  $\pm 1200$  mm, rotation:  $\pm 180^\circ$ ). This highlights the proposed design's potential for effective endovascular intervention through simultaneous control of commercially available instruments, which facilitates easy adoption by clinicians.

## II. DESIGN REQUIREMENTS

Our design focuses on creating a compact, portable 4-DoF robot capable of precisely actuating a wide range of commercially available endovascular instruments, which vary considerably in diameter. Considering the diversity of cardiovascular interventions and instruments in use, it must independently actuate the rotation and translation of guidewires with diameters ranging from  $\varnothing 0.33$  to  $\varnothing 1$  mm and catheters ranging from 5 and 9F with a minimal footprint to prevent physical interference with clinician's operations. The drive mechanisms should provide a minimal force and torque resolution of 20.0 mN and 0.04 mNm, respectively, which are considered thresholds for safe and effective manipulation of instruments within delicate vascular tissues. At the higher end, instrument actuation forces and torques in the



**Fig. 3.** 4-DoF endovascular robot is compact and versatile, accommodating instruments of different diameters. All actuating modules are independently controllable, allowing synchronous translation and rotation of the guide catheter and guidewire without constraints. This feature mimics the clinician's hand cues, improving robot adaptability and enhancing procedural efficiency.

range of  $\pm 2\text{N}$  and  $\pm 4.5\text{ mNm}$  are necessary for advancing, retracting, or steering catheters safely [38]. The standard femoral entry point in cardiovascular procedures demands instrument translation of at least 1200 mm to reach the heart chambers, with a desired resolution of  $\pm 1\text{ mm}$  to facilitate effective treatments [15], [39].

### III. MECHATRONICS DESIGN

This section details the mechatronics development of our teleoperable robot, detailing its compact architecture, its 2-DoF guide catheter actuation module and 2-DoF guidewire actuation module, and its electronics module.

#### A. Portable and Compact Architecture

As illustrated in Fig. 2, the robot's design comprises a three-layered architecture including top, middle, and bottom modules to actuate endovascular instruments. The hallmark of this design lies in the S-shaped curving and threading of instruments across these actuation layers, without kinking, based on the stiffness and geometric features [40], [41], [42], [43] to significantly reduce the system's footprint. As shown in Fig. 3, the robot's top layer comprises the guide catheter rotation (DoF #1) and translation (DoF #2) actuation modules. The middle layer incorporates the guidewire rotation and translation modules (DoFs #3 and #4), and provides space to accommodate a microcatheter insertion module. The bottom layer houses a custom printed circuit board (PCB) and portable battery.

#### B. Design of the 2-DoF Guide Catheter Module

This module was developed to address the critical barrier of state-of-the-art robotic procedures, where clinicians need

frequent robotic-to-manual procedural conversions due to the robot's limited adaptability to different guide catheter diameters. As illustrated in Fig. 2, the 2-DoF guide catheter actuation capabilities (rotation—DoF #1 and translation—DoF #2) imitates manual procedure capabilities via a rotatable Y-connector (80395, Qosina, USA) to facilitate dye and drug delivery through a wide range of guide catheter diameters. The direct drive, brushless dc (BLDC) motor (RMD-L-4010, MyActuator) and 1.5-mm pitch lead screw translation platform enables precise motion control with a range of 300 mm ( $\pm 0.5\text{ mm}$ ). The relationship between the motor angle and the axial translation is shown as follows:

$$X_c(t) = \beta \cdot \theta_m(t) \quad (1)$$

$$= \frac{l}{2\pi} \cdot \theta_m(t) \quad (2)$$

where  $\beta$  represents the lead screw angle ( $^\circ$ ),  $l$  denotes the thread lead (in millimeter),  $\theta_m$  is the motor angle input ( $\pm 0.3^\circ$ ) for platform translation (in millimeter), and  $X_c$  (in millimeter) denotes the advancement/retraction of the catheter as a function of time  $t$  (seconds). The guide catheter rotation module incorporates a second BLDC motor with a spur gear train (2:1 gear ratio) to achieve  $360^\circ$  RoM ( $\pm 0.3^\circ$ ).

#### C. Design of 2-DoF Guidewire Module

The roller-drive module design facilitates the 2-DoF manipulation of guidewires (i.e., rotation DoF #3 and translation DoF #4) of varying diameters and lengths. As shown in Fig. 2, it incorporates an adjustable friction wheel mechanism to facilitate guidewire insertion and retraction. The instrument translation mechanism consists of an active roller coupled with a motor to feed the guidewire continuously in the axial direction, with

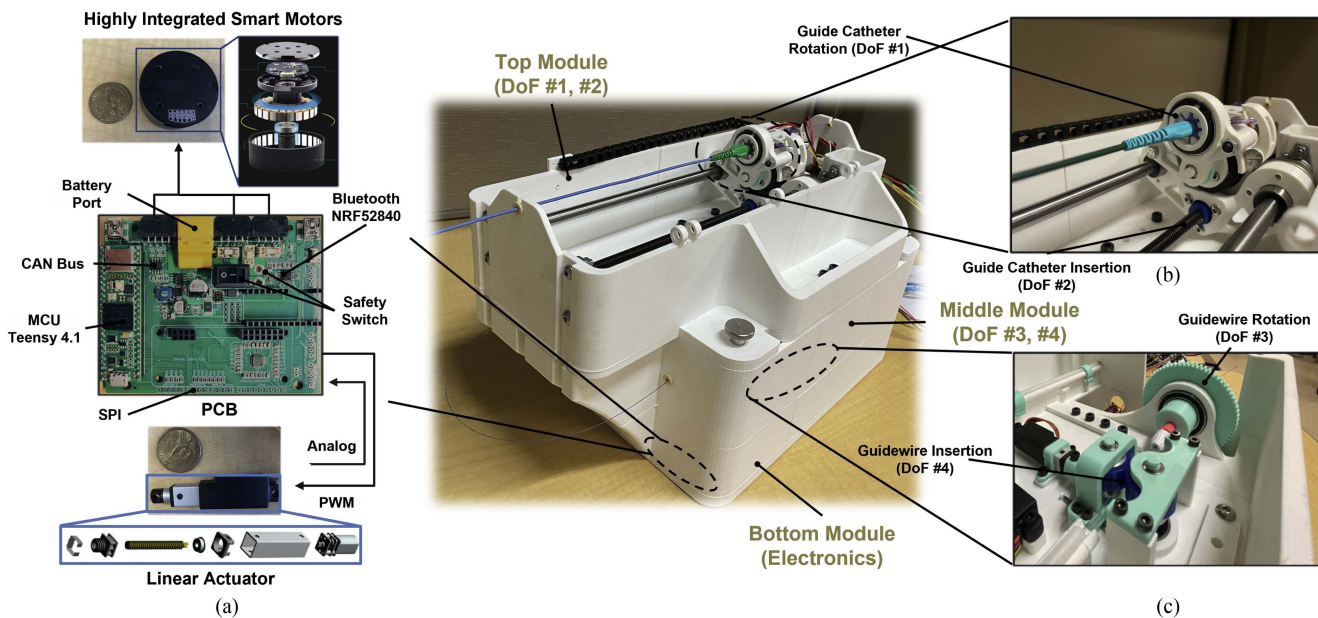


**Fig. 4.** Prototype of a 4-DoF catheter robot that incorporates a 2-DoF guide catheter module and 2-DoF guidewire module, along with compact electronics. (a) Our customized PCB enables communication with integrated smart motors (with fully integrated motor drivers and encoders) via CAN bus protocol. (b) Guide catheter actuation module (DoFs # 1 and # 2) is stacked on the top layer. (c) Guidewire actuation module (DoFs # 3 and # 4) is stacked on the middle layer.

an ROM of more than 1200 mm ( $\pm 0.5$  mm). A linear actuator (L12-10-50-6-P, Actuonix Motion Devices) provides pretension on the guidewire by manipulating the passive roller base through a spring connection to adapt to different guidewire diameters. The instrument rotation platform uses a COTS torquer device (97327/97360, Qosina, USA) and spur gear train to facilitate  $360^\circ$  ( $\pm 0.3^\circ$ ) of guidewire rotation. The axial displacement is calculated as follows:

$$X_g(t) = \frac{1}{2} \cdot D_r \cdot \theta_m(t) \quad (3)$$

where  $X_g$  represents the axial motion of the guidewire (in millimeter),  $D_r$  denotes the diameter of the roller (in millimeter), and  $\theta_m$  is motor rotation angle input ( $^\circ$ ).

#### D. Electronics Design

Customized electronics enable high-fidelity, high-bandwidth communication between the controller and actuation units. The five direct-drive BLDC motors facilitate high-resolution, high-bandwidth control of the instrument outputs (e.g., positional accuracy and insertion force). Furthermore, customized PCBs incorporate a Teensy 4.1 microcontroller (PJRC, USA) and controller area network (CAN) transceivers that enable low-level control at high bandwidths.

**1) Direct Drive Motors:** The direct drive motors are efficient and compact (40 mm in diameter, 28 mm in height, and 92 g in weight), as illustrated in Fig 4(a). These compact gearless motors feature built-in drivers and incremental optical encoders to provide a nominal torque output of 0.15 Nm (peak torque: 0.33 Nm, speed: 1120 r/min) with an input voltage range of 8–24 V. The motor drivers enable torque loop, speed loop, and position loop control. Each motor unit includes an electronic

control unit to establish and maintain real-time communication with the microcontroller via the CAN bus protocol. Adopting this CAN bus protocol enables simultaneous real-time control of multiple motors at varying operating frequencies. The integrated encoder delivers 14 bits of rotor resolution, ensuring high-fidelity position feedback for the precise placement of instruments within the vasculature.

**2) Grip Actuator:** This small-footprint linear actuator (L12-10-50-6-P, Actuonix Motion Devices) maintains a robust grip on the instruments. This actuator incorporates a micro BLDC motor into a lead screw mechanism, enabling the effective conversion of rotational motion into linear translation with minimal back drivability. Its 50:1 gear ratio provides a repeatability of 0.1 mm via potentiometer position feedback, a maximum stroke length of 10 mm, and a maximum force of 22 N, with a back drive force of 12 N. The low back-drivability of these actuators enhances mechanism robustness and mitigates radial/tangential slip of instruments. As illustrated in Fig. 5, the passive roller incorporates a biasing spring to adapt to various guidewire diameters. As the extended length of the linear actuator can be tailored in real-time (via commands from the microcontroller) and the distance between the rollers and the diameter of guidewires are known, the spring assists in establishing adequate force for the friction roller to actuate these thin guidewires and ensure adequate grip.

**3) CAN Bus Communication Electronics:** Our customized two-layer PCB design establishes high-fidelity, high-bandwidth communication between the microcontroller and all five actuators, as illustrated in Fig. 4(a), and is expandable up to nine actuators. Its compact geometry (100 mm length by 85 mm width) greatly assists in reducing the footprint of the robot. The system microcontroller (a Teensy 4.1) regulates five direct

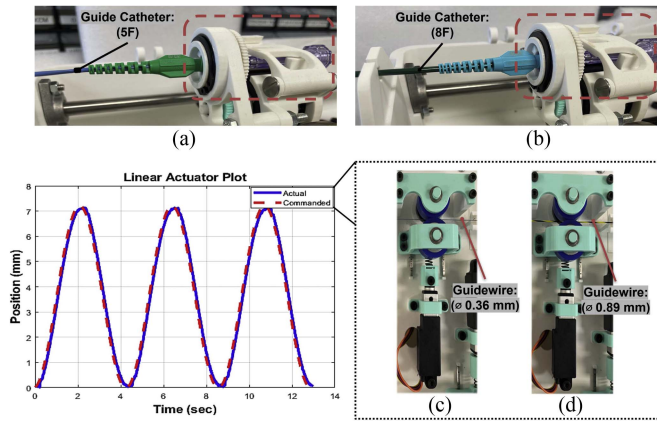


**Fig. 5.** Clamping feature of the versatile guide catheter module incorporates off-the-shelf rotatable y-connectors into the driven gear to actuate catheters. (a) Module's compatibility with a 5-Fr guide catheter. (b) Module with the 8-Fr guide catheter; see Fig. 2. Pretension guidewire module facilitates accurate grip by tailoring the linear actuator shaft to accommodate versatile guidewire diameters. (c) Accurate retention on the 1 Fr ( $\varnothing$  0.36 mm) guidewire. (d) 3 Fr ( $\varnothing$  0.89 mm).

drive motors via CAN bus protocol and two linear actuators via pulsewidth modulation output and analog input. Furthermore, the PCB design can also accommodate different communication protocol electronic units (such as I2C, SPI, UART, USB) and holds a battery port to power all electronic units by reducing the necessity for numerous channels. Finally, the 22-V battery powers the PCB (including the microcontroller and all the actuators) for nearly 5 h, promoting the robot's accessibility for telemanipulation.

#### IV. EXPERIMENTS AND RESULTS

We conducted a variety of benchtop experiments to characterize the performance and versatility of instrument manipulation, specifically the following:

- 1) the mechanical versatility to drive guide catheters and guidewires with different and clinically relevant diameters;
- 2) the precise control of tip translation and rotation, and actuation force and torque, to meet clinical requirements without damaging delicate tissues.

Position tracking experiments evaluated the system's tracking accuracy and repeatability, while insertion force characterization tests were conducted to ensure the robot could actuate a range of instruments and achieve the desired insertion forces required for cardiovascular interventions.

##### A. Position Tracking Experiments

1) *Task-Space Tracking*: Because simultaneous manipulation (i.e., rotation and linear translation) of the guidewire and guide catheter is critical for most cardiovascular procedures, we conducted a series of simultaneous task-space position tracking experiments. We employed commercial guide catheters (a 5-F H74939228090 CONVEY FL5 and an 8-F M001198660 MACH 1 19866, Boston Scientific, USA) and guidewires (a 0.36 mm  $\times$  300 cm CHOICE PT floppy with straight tip and a 0.89 mm  $\times$

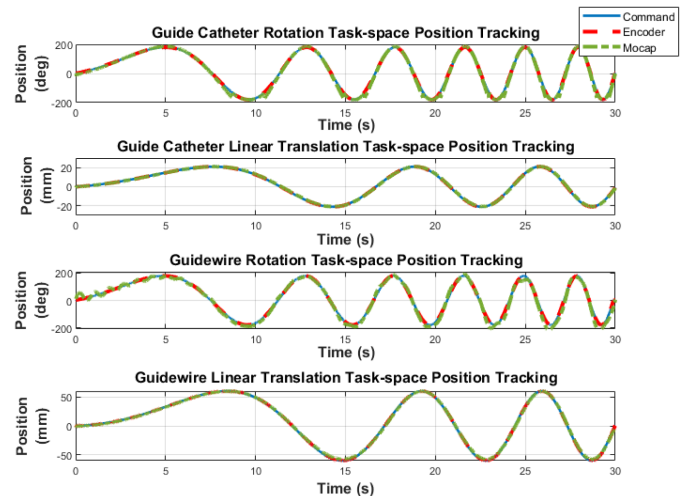


**Fig. 6.** Simultaneous swept sine position tracking of the guidewire and guide catheter. The first two plots illustrate the guide catheter position tracking with sine sweep input, rotation (DoF # 1): 0.02–0.2 Hz and 180° amplitude and linear translation (DoF # 2): 0.01–0.1 and 20-mm amplitude. The bottom two plots demonstrate the guidewire rotation (DoF # 3): 0.02–0.2 Hz and 180° amplitude and linear translation (DoF # 4): 0.002–0.2 Hz and 60-mm amplitude.

450 cm Hydra Jagwire stiff with straight tip, Boston Scientific, USA) to evaluate tracking performance. As shown in Fig. 6, The position-tracking experiments utilized the smallest diameter instruments (i.e., the 5-F guide catheter and 0.36-mm guidewire) and included simultaneous rotation and translation of both the guide catheter and guidewire. Specifically, the guide catheter tracking utilized a swept sine rotation reference of 0.02–0.2 Hz with an amplitude of 180°, while its linear translation tracked a swept sine wave reference of 0.01–0.1 Hz with an amplitude of 20 mm. Similarly, simultaneous guidewire rotation and translation experiments involved swept sine rotation references (0.02–0.2 Hz with an amplitude of 180°) and translation references (0.002–0.2 Hz with an amplitude of 60 mm). These swept sine experiments facilitated the examination of the controllable bandwidths of all actuation modules. The guide catheter and guidewire rotation modules were studied by operating the rotatory modules between 7.2°/s and 72°/s. In contrast, the guide catheter linear translation module was commanded between 0.4 and 4 mm/s, and the guidewire linear translation module was commanded between 0.24 and 24 mm/s.

Four motion capture cameras (Qualisys Miquis M5, Sweden) were employed to precisely monitor the instrument position in the benchtop setting. Four reflective markers were attached around the instrument to quantify the real-time linear and rotational motion of both the guidewire and guide catheter. The reflective marker data was acquired at 100 Hz to track the instrument movements with high fidelity. Because the endovascular instruments were subjected to axial and torsional mechanics, task-space measurements (angular and linear positions of the instrument tip) exhibited low-amplitude oscillations and deviations with respect to the joint-space actuator commands. These differences were quantified via root-mean-squared-error

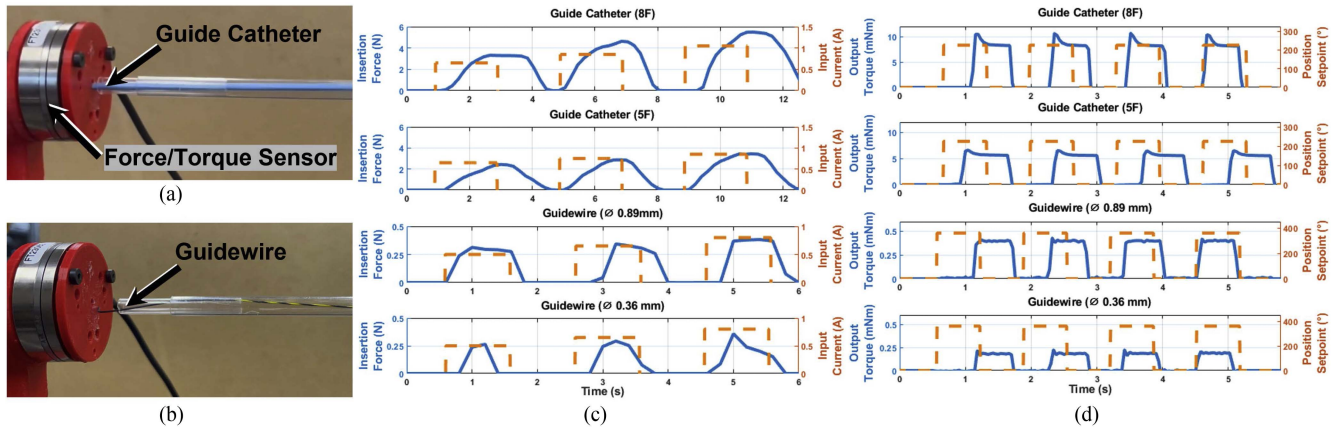


**Fig. 7.** Measured actuation force and torque profiles for different diameter instruments. (a) Experimental setup for guide catheter force and torque measurements. (b) Experimental setup for guidewire force and torque measurements. (c) Measured force profiles, where orange indicates commanded motor current, and blue represents measured forces. Input current amplitudes of 0.65, 0.80, and 1.05 A were used for the guide catheter drive motors, with step periods of 2.5 s. For the guidewires, motor current step amplitudes of 0.50, 0.65, and 0.80 A were used with step periods of 0.75 s. Peak guide catheter force measurements were 5.49 N (for 8 F) and 3.44 N (5 F), peak guidewire force measurements were 0.38 N (for  $\varnothing$  0.89 mm) and 0.35 N (for  $\varnothing$  0.36 mm). (d) Measured torque profiles, where orange indicates commanded position setpoint and blue represents measured torques. Peak guide catheter torque measurements were 10.61 mNm (for 8 F) and 6.55 mNm (5 F), and peak guidewire torque measurements were 0.42 mNm (for  $\varnothing$  0.89 mm) and 0.22 mNm (for  $\varnothing$  0.36 mm).

(RMSE) analysis to be  $10.3^\circ$  and 0.31 mm, respectively. Furthermore, guidewire rotation and linear translation data reveal differences of approximately  $6.9^\circ$  and 0.9 mm, respectively. These results demonstrate the robot's ability to enable coupled manipulation of commercially available instruments with the intuitiveness of instrument control via joint-space commands.

### B. Instrument Insertion Force and Torque Characterization

We evaluated the robot's force and torque capabilities using the same commercial guide catheters and guidewires. Specifically, we quantified the actuation performance of both the guide catheter and guidewire translation modules via a series of scaled current step responses. Although peak insertion forces during PCI vary significantly depending on catheter type, procedural technique, and patient anatomy, published ranges of 0.1 N to more than 1.5 N are common [15], [39]. To explore the high end of this range, input current amplitudes of 0.65, 0.80, and 1.05 A were used for the guide catheter drive motors, with step periods of 2.5 s. For the guidewires, motor current step amplitudes of 0.50, 0.65, and 0.80 A were used with step periods of 0.75 s. The experimental setup utilized a six-axis force and torque transducer (Nano43 US-2-1, ATI Industrial Automation, USA) to characterize insertion forces and torques at the device tips. The force and torque sensor was situated at a distance of 700 mm from the robot, and the robot was commanded to drive the instruments through 6-mm diameter clear plastic tubing (to mimic endovascular support, Fig. 7).

As shown in Fig. 7, a peak insertion force of 5.49 N was observed while actuating the 8-F guide catheter with a drive motor current of 1.05 A. Peak force measurements for the 5-F guide catheter were 3.44 N. Roller drive-based guidewire translation produced peak forces of 0.37 N for the  $\varnothing$  0.89-mm guidewire and 0.35 N for the  $\varnothing$  0.36-mm guidewire, both at

drive motor currents of 0.80 A. The experiment conducted on a  $\varnothing$  0.36-mm guidewire revealed that the quantified insertion force decreased slightly over a period due to induced bending of the instrument tip, as illustrated in Fig. 7. Also shown in Fig. 7 are measured torque profiles for the 5- and 8-F guide catheters and the  $\varnothing$  0.36-mm and  $\varnothing$  0.89-mm guidewires. Peak guide catheter torque measurements were 10.61 mNm (8 F) and 6.55 mNm (5 F), both for commanded position setpoints of  $225^\circ$ . Peak guidewire torque measurements were 0.42 mNm ( $\varnothing$  0.89 mm) and 0.22 mNm ( $\varnothing$  0.36 mm), both for commanded position setpoints of  $360^\circ$ . These torque profiles were repeatable and exhibited less relaxation than the force profiles.

Because large insertion force amplitudes could pose risks to delicate tissues, additional experiments were conducted at the low end of the controllable insertion force range. For these experiments, the 8-F guide catheter was actuated using a setpoint position input of 0.25 mm, resulting in very low but repeatable insertion forces (peak: 42.2 mN, average: 22.5 mN) with an average actuation current of 0.21 A. Similarly, a  $\varnothing$  0.89-mm guidewire was commanded with a position setpoint of 3.78 mm, again resulting in low but repeatable insertion forces (peak: 25.6 mN, average: 15.9 mN), with an average actuation current of 0.19 A (see Fig. 8).

### C. Experimental PCI in a Human Heart Phantom

To demonstrate the clinical potential of our catheter robot, we conducted experimental PCI using a transparent human heart phantom. The heart phantom geometry was derived from clinical scans and converted to solid model format (TurboSquid.com, [44]) and 3-D printed in clear resin (FormLabs Form 3, USA). As shown in Fig. 9, a guidewire (0.89 mm  $\times$  450 cm Hydra Jagwire stiff guidewire with straight tip, Boston Scientific, USA) was robotically introduced via the left subclavian artery into the aorta at a rate of approximately 1 mm/s

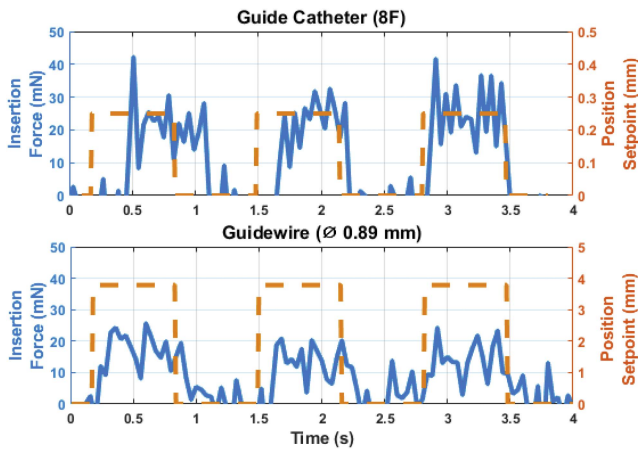


**Fig. 8.** Minimum repeatable insertion forces for a 8-F guide catheter and a 3F guidewire. The guide catheter results illustrate the forces (peaking at 42.2 mN, average 22.5 mN) achieved by translating the instrument with a position setpoint of 0.25-mm amplitude, drawing a current of 0.21 A (root mean square). Similarly, the guidewire was commanded with a position setpoint of 3.78 mm; this resulted in quantifying insertion forces (peak: 25.6 mN, average: 15.9 mN), drawing a current of 0.19 A.

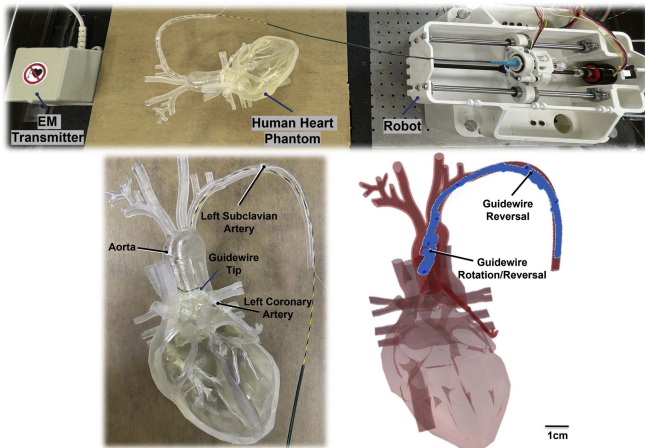


**Fig. 9.** Robotic guidewire deployment in a human heart phantom to simulate PCI. (Top) Experimental setup showing catheter robot, heart phantom, and transmitter for 3-D EM tracker system. (Bottom left) Transparent 3-D-printed heart phantom, with guidewire robotically advanced via the left subclavian artery into the aorta and advanced to the entrance of the left coronary artery. (Bottom right) Measured 3-D position tracking of guidewire tip (shown as blue sample points) overlaid on the solid model of the heart phantom, showing instrument trajectory. Reversals and rotations of the guidewire tip are visible: these enabled passage through tortuous vessels and around vascular obstructions.

and advanced to the entrance of left coronary artery. Real-time tracking of the guidewire tip was accomplished using an attached 6-DOF electromagnetic tracking sensor (TrakSTAR MRT, NDI, ON, Canada), which was sampled at 100 Hz to acquire the task space position and orientation. The resulting guidewire trajectory is presented in Fig. 9, showing accurate and effective guidewire deployment throughout this simulated PCI procedure.

## V. CONCLUSION

In this article, we have presented the design, development, and experimental characterization of a portable and versatile robot with a compact footprint that can precisely manipulate a range of off-the-shelf instruments to achieve desired motion specifications. This work also introduced detailed modeling of the friction roller drive actuation system to quantify the nonlinear relationship between roller grip and instrument insertion forces, which helps mitigate slippage. The joint-space tracking results demonstrated the robot's capability to actuate all four modules simultaneously to achieve coupled instrument manipulation (i.e., rotation and linear translation). Guidewire and guide catheter modules reported low RMS error (linear  $\leq 0.09$  mm, rotation  $\leq 0.014^\circ$ ). Our task-space instrument swept sine tracking results demonstrated the robot's ability to manipulate the guidewire and guide catheter at various intervention speed ranges with an intuitive correspondence between the joint-space commands and task-space movements. These task-space position tracking experiments involve simultaneous manipulation of the instruments in a benchtop setting. Coupled guidewire rotation and translation were investigated by operating the rotational drive module between 7.2 and  $72^\circ/\text{s}$ , and the translational drive module between 0.24 and 24 mm/s. Similarly, coupled guide catheter rotation and translation were studied by commanding the actuation modules at rates between 7.2 and  $72^\circ/\text{s}$ , and 0.4 and 4 mm/s, respectively. Due to the flexural mechanics of the instruments, differences in rotation tracking between the joint space and task space were observed, not exceeding  $10.3^\circ$ . Likewise, instrument linear translation results exhibited submillimeter differences of  $\leq 0.9$  mm. These minimal disparities between joint-space commands and task-space movements demonstrate our versatile mechanism's ability to achieve high accuracy and repeatability with a compact design.

Mechanical versatility experiments involved actuation of the smallest and largest instrument diameters (i.e., guidewire and guide catheter) to characterize the instrument's insertion force capabilities. These quantified force results demonstrated the ability of the versatile translation modules (i.e., guidewire and guide catheter insertion modules) to effectively drive a range of instruments and achieve the requisite insertion forces of most cardiovascular procedures [38]. The peak guide catheter driving force was quantified to be 5.49 N, with a peak guidewire insertion force of 0.37 N, with torque commands lower than the drive motor's peak capability (thus, our robot has the potential to achieve even higher insertion forces). One limitation of the current study is that we evaluated our robot only in benchtop settings. Thus, extensive testing using vascular phantoms, explanted vascular tissues, and in vivo procedures should be conducted to fully investigate and characterize the robot's full potential in anatomical settings.

In conclusion, our robot design features a portable architecture that is achieved by curving the instruments through multiple actuation module layers, making it compact and accessible to diverse clinical settings. Our robot's versatile actuation modules facilitate adaptation to diverse off-the-shelf instruments and enable simultaneous manipulation of instruments with greater

accuracy and repeatability. The versatility feature of our modules can potentially empower the robot to execute diverse cardiovascular procedures. While our current robot is not designed to facilitate standard instrument sterilization techniques (autoclaves, ethylene oxide, etc.), future work will focus on a more modular design, where the drive mechanisms that directly contact the guide wires and guide catheters will be contained in a removable cartridge suitable for sterilization. Furthermore, the modular design of our catheter robot requires that a nominal length of guidewire and catheter (approximately 50 cm) reside within the drive modules so that even procedures requiring only 50 cm of stroke will require instruments of approximately 100 cm in length. A focus of future research will be to reduce this nominal drive module length.

### ACKNOWLEDGMENT

The authors would like to thank B. Liu, S. Jernigan, and Dr. M. Chen for their valuable assistance in carrying out the robot experiments. The authors would also like to thank B. Woodleaf (ATI) for his assistance with the actuation force and torque measurements.

*Authors' Contributions:* Nikhil Tej Kantu: Writing of original draft and editing, conceptualization, methodology, and investigation. Weibo Gao: Writing of review and editing, electronics development, and project logistical support.

### REFERENCES

- [1] G. A. Roth et al., "Global burden of cardiovascular diseases and risk factors, 1990–2019: Update from the GBD 2019 study," *J. Amer. College Cardiol.*, vol. 76, no. 25, pp. 2982–3021, 2020.
- [2] E. Brilakis, *Manual of Percutaneous Coronary Interventions: A Step-By-Step Approach*. Cambridge, MA, USA: Academic, 2020.
- [3] T. Walther et al., "Transapical aortic valve implantation: Step by step," *Ann. Thoracic Surg.*, vol. 87, no. 1, pp. 276–283, 2009.
- [4] M. D. O'Neill et al., "The stepwise ablation approach for chronic atrial fibrillation—Evidence for a cumulative effect," *J. Interventional Cardiac Electrophysiol.*, vol. 16, pp. 153–167, 2006.
- [5] E. L. Chaikof et al., "Identifying and grading factors that modify the outcome of endovascular aortic aneurysm repair," *J. Vasc. Surg.*, vol. 35, no. 5, pp. 1061–1066, 2002.
- [6] Q.-H. Tang, J. Chen, C.-F. Hu, and X.-L. Zhang, "Comparison between endovascular and open surgery for the treatment of peripheral artery diseases: A meta-analysis," *Ann. Vasc. Surg.*, vol. 62, pp. 484–495, 2020.
- [7] A. K. Thukkani and S. Kinlay, "Endovascular intervention for peripheral artery disease," *Circulation Res.*, vol. 116, no. 9, pp. 1599–1613, 2015.
- [8] J. Chakravarti and S. V. Rao, "Robotic assisted percutaneous coronary intervention: Hype or hope?," *J. Amer. Heart Assoc.*, vol. 8, no. 13, 2019, Art. no. e012743.
- [9] N. Kaneko, C. Beaman, T. Imahori, A. Takayanagi, H. Saber, and S. Tateshima, "In vitro comparison of manual and robotic endovascular thrombectomy for acute ischemic stroke," *Interventional Neuroradiol.*, 2023, Art. no. 15910199231206315.
- [10] E. M. Khan et al., "First experience with a novel robotic remote catheter system: Amigo™ mapping trial," *J. Interventional Cardiac Electrophysiol.*, vol. 37, pp. 121–129, 2013.
- [11] M. E. Abdelaziz et al., "Toward a versatile robotic platform for fluoroscopy and MRI-guided endovascular interventions: A pre-clinical study," in *Proc. IEEE/RSJ Int. Conf. Intell. Robots Syst.*, 2019, pp. 5411–5418.
- [12] W. Saliba et al., "Atrial fibrillation ablation using a robotic catheter remote control system: Initial human experience and long-term follow-up results," *J. Amer. College Cardiol.*, vol. 51, no. 25, pp. 2407–2411, 2008.
- [13] Z.-Q. Feng, G.-B. Bian, X.-L. Xie, Z.-G. Hou, and J.-L. Hao, "Design and evaluation of a bio-inspired robotic hand for percutaneous coronary intervention," in *Proc. IEEE Int. Conf. Robot. Automat.*, 2015, pp. 5338–5343.
- [14] Y. Kim et al., "Telerobotic neurovascular interventions with magnetic manipulation," *Sci. Robot.*, vol. 7, no. 65, 2022, Art. no. eabg9907.
- [15] P. Bergman, S. J. Blacker, N. Kottenstette, O. Saber, and S. Sokhanvar, "Robotic-assisted percutaneous coronary intervention," in *Handbook of Robotic and Image-Guided Surgery*. Amsterdam, The Netherlands: Elsevier, 2020, pp. 341–362.
- [16] H. Su et al., "Piezoelectrically actuated robotic system for MRI-guided prostate percutaneous therapy," *IEEE/ASME Trans. Mechatron.*, vol. 20, no. 4, pp. 1920–1932, Aug. 2015.
- [17] G. Li et al., "Robotic system for MRI-guided stereotactic neurosurgery," *IEEE Trans. Biomed. Eng.*, vol. 62, no. 4, pp. 1077–1088, Apr. 2015.
- [18] H. Su, G. Li, D. C. Rucker, R. J. Webster III, and G. S. Fischer, "A concentric tube continuum robot with piezoelectric actuation for MRI-guided closed-loop targeting," *Ann. Biomed. Eng.*, vol. 44, pp. 2863–2873, 2016.
- [19] Z. Guo et al., "Techniques for stereotactic neurosurgery: Beyond the frame, toward the intraoperative magnetic resonance imaging-guided and robot-assisted approaches," *World Neurosurg.*, vol. 116, pp. 77–87, 2018.
- [20] Y. Chen, I. Godage, H. Su, A. Song, and H. Yu, "Stereotactic systems for MRI-guided neurosurgeries: A state-of-the-art review," *Ann. Biomed. Eng.*, vol. 47, pp. 335–353, 2019.
- [21] H. Su, M. Zervas, G. A. Cole, C. Furlong, and G. S. Fischer, "Real-time MRI-guided needle placement robot with integrated fiber optic force sensing," in *Proc. IEEE Int. Conf. Robot. Autom.*, 2011, pp. 1583–1588.
- [22] H. Su et al., "MRI-guided concentric tube continuum robot with piezoelectric actuation: A feasibility study," in *Proc. IEEE Int. Conf. Robot. Autom.*, pp. 1939–1945.
- [23] H. Su, W. Shang, G. Li, N. Patel, and G. S. Fischer, "An MRI-guided telesurgery system using a Fabry-Perot interferometry force sensor and a pneumatic haptic device," *Ann. Biomed. Eng.*, vol. 45, pp. 1917–1928, 2017.
- [24] H. Su et al., "Fiber-optic force sensors for MRI-guided interventions and rehabilitation: A review," *IEEE Sensors J.*, vol. 17, no. 7, pp. 1952–1963, Apr. 2017.
- [25] H. Su et al., "State of the art and future opportunities in MRI-guided robot-assisted surgery and interventions," *Proc. IEEE*, vol. 110, no. 7, pp. 968–992, Jul. 2022.
- [26] J. H. Crews and G. D. Buckner, "Design optimization of a shape memory alloy-actuated robotic catheter," *J. Intell. Mater. Syst. Structures*, vol. 23, no. 5, pp. 545–562, 2012.
- [27] J. H. Wiest and G. D. Buckner, "Path optimization and control of a shape memory alloy actuated catheter for endocardial radiofrequency ablation," *Robot. Auton. Syst.*, vol. 65, pp. 88–97, 2015.
- [28] C. Abah, R. Chitale, and N. Simaan, "Image-guided optimization of robotic catheters for patient-specific endovascular intervention," in *Proc. Int. Symp. Med. Robot.*, 2021, pp. 1–8.
- [29] J. J. Zhou et al., "The CathPilot: A novel approach for accurate interventional device steering and tracking," *IEEE/ASME Trans. Mechatron.*, vol. 27, no. 6, pp. 5812–5823, Dec. 2022.
- [30] S. Guo et al., "A novel robot-assisted endovascular catheterization system with haptic force feedback," *IEEE Trans. Robot.*, vol. 35, no. 3, pp. 685–696, Jun. 2019.
- [31] G. Bassil et al., "Robotics for catheter ablation of cardiac arrhythmias: Current technologies and practical approaches," *J. Cardiovasc. Electrophysiol.*, vol. 31, no. 3, pp. 739–752, 2020.
- [32] H. Rafii-Tari, C. J. Payne, and G.-Z. Yang, "Current and emerging robot-assisted endovascular catheterization technologies: A review," *Ann. Biomed. Eng.*, vol. 42, pp. 697–715, 2014.
- [33] N. V. Belikov, I. V. Khaydukova, I. E. Poludkin, and A. S. Borde, "Evolution and current state of robotic catheters for endovascular surgery: A comprehensive review," *Int. J. Eng. Sci. Technol.*, vol. 57, 2024, Art. no. 101789.
- [34] B. Ren, Y. Zhao, J. Zhang, H. Li, K. Li, and J. Zhang, "The critical technologies of vascular interventional robotic catheterization: A review," *IEEE Sensors J.*, vol. 23, no. 24, pp. 30051–30069, Dec. 2023.
- [35] T. Wenderow et al., "Robotic catheter system," U.S. Patent 10 987 491, Apr. 27, 2021.
- [36] H. Saber, C. Beaman, J. Morales, D. Kimball, N. Kaneko, and S. Tateshima, "Full robotic endovascular treatment for various head and neck hemorrhagic lesions," *Interventional Neuroradiol.*, vol. 30, 2023, Art. no. 15910199231169417.
- [37] D. Steitieh, N. Sharma, and H. S. Singh, "How technology is changing interventional cardiology," *Curr. Cardiovasc. Risk Rep.*, vol. 16, no. 1, pp. 1–10, 2022.
- [38] D. Ilic, T. Moix, B. Fracheboud, H. Bleuler, and M. I. Vecerina, "A haptic interface for interventional radiology," in *Proc. IEEE Int. Conf. Robot. Autom.*, 2005, pp. 2933–2937.

- [39] J. Bonatti, G. Vetrovec, C. Riga, O. Wazni, and P. Stadler, "Robotic technology in cardiovascular medicine," *Nature Rev. Cardiol.*, vol. 11, no. 5, pp. 266–275, 2014.
- [40] P. Poli, A. Scocca, F. Di Puccio, G. Gallone, L. Angelini, and E. M. Calabrò, "A comparative study on the mechanical behavior of polyurethane PICCs," *J. Vasc. Access*, vol. 17, no. 2, pp. 175–181, 2016.
- [41] "I. Mechanical properties of catheters," *Acta Radiologica: Diagnosis*, vol. 4, no. sup260, pp. 11–22, 1966.
- [42] W. Schummer, S. Trommer, F. Kleemann, and C. Schummer, "Mechanical properties of Seldinger guidewires," *J. Vasc. Access*, vol. 15, no. 6, pp. 507–513, 2014.
- [43] M. Fedel et al., "Functional properties and performance of new and reprocessed coronary angioplasty balloon catheters," *J. Biomed. Mater. Res., Appl. Biomaterials*, vol. 78, pp. 364–372, 2006.
- [44] *TurboSquid*, "Heart anatomical cross-section 3D model," 2024. Accessed: Dec., 11, 2024. [Online]. Available: <https://www.turbosquid.com/3d-models/3d-model-heart-anatomical-cross-section-1424032>



**Nikhil Tej Kantu** (Student Member, IEEE) received the Bachelors of Technology degree in mechanical engineering from BML Munjal University, Kapriwas, India, in 2019, and the M.S. degree in robotics and automation engineering from the State University of New York, Buffalo, NY, USA, in 2022. He is currently working toward the Ph.D. degree in mechanical engineering with North Carolina State University, Raleigh, NC, USA.

He was a Graduate Research Assistant with AI-based WEARable Robotic Lab, Buffalo, from 2020 to 2022. He was a robotics Researcher with CSIR-Central Scientific Instrument Organization, Chandigarh, India, in 2019. His research interests include surgical robotics, rehabilitation robotics, human–robot interactions, and biomechanics.



**Weibo Gao** (Graduate Student Member, IEEE) received the B.S. degree in mechanical engineering from Xi'an Jiaotong University, Xi'an, China, in 2017, and the M.S. degree in mechanical engineering from the University of Pittsburgh, Pittsburgh, PA, USA, in 2019. He is currently working toward the Ph.D. degree in mechanical engineering with North Carolina State University, Raleigh, NC, USA, under the supervision of Prof. H. Su.

His current research interests include design and control of medical robots.



**Nitin Srinivasan** received the B.Tech. degree in mechanical engineering from the Dayananda Sagar College of Engineering, Bangalore, India, in 2021, and the M.S. degree in mechanical engineering from the North Carolina State University, Raleigh, NC, USA, in 2024.

He is currently working as a Research Engineer with the Biomechanics and Intelligent Robotics Lab, North Carolina State University, under the supervision of Prof. H. Su. His research interests include mechanism design and medical robots.



**Gregory D. Buckner** (Member, IEEE) received the B.S. degree in mechanical engineering from Louisiana State University, Baton Rouge, LA, USA, in 1986, the M.S. degree in mechanical engineering from Virginia Polytechnic Institute, Blacksburg, VA, USA, in 1987, and the Ph.D. degree in mechanical engineering from the University of Texas at Austin, Austin, TX, USA, in 1996.

He is a Professor of mechanical and aerospace engineering with North Carolina State University, Raleigh, NC, USA, and a Faculty Affiliate with the University of North Carolina at Chapel Hill/North Carolina State University Joint Department of Biomedical Engineering, Raleigh. His current research interests include the design and control of electromechanical systems, with applications to medical and automotive technologies.

Dr. Buckner was the recipient of the Faculty Early Career Development (CAREER) Award from the National Science Foundation, the New Faculty Research Award from the American Society for Engineering Education, the Distinguished Undergraduate Professor Award from the North Carolina State University Alumni Association, and the Ralph R. Teetor Educational Award from the Society of Automotive Engineers. He is an Associate Editor for *ASME Journal of Dynamic Systems, Measurement and Control*.



**Hao Su** (Senior Member, IEEE) received the B.S. degree in automation from the Harbin Institute of Technology, Harbin, China, in 2006, the M.S. degree in mechanical engineering from the State University of New York University, Buffalo, NY, USA, in 2008, and the Ph.D. degree in mechanical engineering from Worcester Polytechnic Institute, Worcester, MA, USA, in 2013.

He was an Associate Professor with North Carolina State University and University of North Carolina at Chapel Hill and a Research Scientist with Philips Research North America and a Postdoctoral Fellow with Harvard University and Wyss Institute for Biologically Inspired Engineering. He is currently an Associate Professor with the Tandon School of Engineering, New York University, Brooklyn, NY, USA.

Dr. Su was the recipient of the National Science Foundation CAREER Award and the Switzer Distinguished Fellowship of the U.S. Department of Health and Human Services. He is a Technical Editor for IEEE/ASME TRANSACTIONS ON MECHATRONICS, an Associate Editor for IEEE ROBOTICS AND AUTOMATION MAGAZINE and *ASME Journal of Mechanisms and Robotics*, and Editorial Advisory Board of the *International Journal of Medical Robotics and Computer-Assisted Surgery*.